A&A 474, 689–700 (2007)
DOI: 10.1051/0004-6361:20078298

Astronomy & Astrophysics

Spectral evolution of non-thermal electron distributions in intense radiation fields

K. Manolakou[1], D. Horns[1], and J. G. Kirk[2]

[1] Institute for Astronomy and Astrophysics Tübingen (IAAT) Sand 1, 72076 Tübingen, Germany
e-mail: horns@astro.uni-tuebingen.de
[2] Max-Planck-Institut für Kernphysik, Saupfercheckweg 1, 69117 Heidelberg, Germany

Received 17 July 2007 / Accepted 4 August 2007

ABSTRACT

Context. Models of many astrophysical gamma-ray sources assume they contain a homogeneous distribution of electrons that are injected as a power law in energy and evolve by interacting with radiation fields, magnetic fields, and particles in the source and by escaping. This problem is particularly complicated if the radiation fields have higher energy density than the magnetic field and are sufficiently energetic that inverse Compton scattering is not limited to the Thomson regime.
Aims. We present a simple, time-dependent, semi-analytical solution to the electron kinetic equation that treats both continuous and impulsive injection, cooling via synchrotron and inverse Compton radiation (taking Klein-Nishina effects into account), and energy-dependent particle escape. We used this solution to calculate the temporal evolution of the multi-wavelength spectrum of systems where energetic electrons cool in intense photon fields.
Methods. The kinetic equation for an arbitrary, time-dependent source function is solved by the method of Laplace transformations. Using an approximate expression for the energy-loss rate that takes synchrotron and inverse Compton losses into account, including Klein-Nishina effects for scattering off an isotropic photon field with either a power-law or black-body distribution, we find explicit expressions for the cooling time and escape probability of individual electrons. This enables the full, time-dependent solution to be reduced to a single quadrature. From the electron distribution, we then construct the time-dependent, multi-wavelength emission spectrum.
Results. We compare our solutions with several limiting cases and discuss the general appearance and temporal behaviour of spectral features (i.e., cooling breaks, bumps, etc.). As a specific example, we model the broad-band energy spectrum of the open stellar association Westerlund-2 at different times of its evolution, and compare it with observations. The model calculation matches the observations for a source with an age greater than $\approx 10^5$ yrs. We predict that the GLAST gamma-ray observatory should easily detect this source.
Conclusions. The technique we present enables simple, computationally efficient, time-dependent models of homogeneous sources to be constructed and compared with multi-wavelength observations.

Key words. gamma rays: theory – radiation mechanisms: non-thermal – stars: Wolf-Rayet – ISM: cosmic rays – open clusters and associations: individual: Westerlund 2

1. Introduction

The discovery of very high-energy (VHE, $E_\gamma > 100$ GeV) gamma rays from many different astrophysical sources (for a recent review see Völk 2006) has motivated the construction of simple, physical models of the emission regions. An important ingredient in such models is the interaction of accelerated leptons with an intense ambient radiation field, especially by inverse Compton scattering. For example, the recent discovery of VHE emission from sources possibly associated with stellar clusters, including Westerlund-2 (Wd-2) (Aharonian et al. 2007), Berk-87 (Abdo et al. 2007), and Cyg OB2 (Aharonian et al. 2002, 2005a), provides evidence of particle acceleration in an environment dominated by hot massive stars driving fast winds, as well as supernova remnants evolving in a dilute, hot medium (Tang & Wang 2005). The detection of VHE gamma-rays from high-mass X-ray binary systems like LS I+61 303 (Albert et al. 2006), LS 5039 (Aharonian et al. 2005b), and PSR B1259-63 (Aharonian et al. 2005c) adds another class of galactic sources where inverse Compton scattering is expected to be an important energy-loss mechanism.

In addition to the VHE emission, these sources show evidence of non-thermal X-ray emission, which is also spatially extended in the case of Wd-2 and Cyg OB2 (Townsley et al. 2005; Horns et al. 2007). Leptonic scenarios have been used both to predict and to model the multi-wavelength spectra (Kirk et al. 1999; Murata et al. 2003; Khangulyan et al. 2007; Hinton & Aharonian 2007), although hadronic models in which the gamma rays are produced in nucleonic collisions also provide a natural explanation (Neronov & Chernyakova 2006; Horns et al. 2007; Bednarek 2007).

Improved modelling of these sources is clearly necessary for a better understanding of the mechanisms at work. However, even with drastic simplifications, such as the assumption of spatial homogeneity, and the ad hoc prescription of a distribution function of injected particles, such models can be quite complicated to construct. Furthermore, the need to investigate a large volume of parameter space makes it important to find computationally efficient algorithms.

The temporal evolution of a non-thermal electron distribution interacting with matter and photon fields has been studied in great detail in the past (see e.g. Ginzburg & Syrovatskii 1964; Felten & Morrison 1966; Blumenthal & Gould 1970; Mastichiadis & Kirk 1997; Sturner et al. 1997). The problem can be described by an integro-differential equation including all relevant energy-loss mechanisms for electrons (e.g. Blumenthal & Gould 1970; Zdziarski 1989; Coppi 1992; Kusunose & Takahara 2005), which is numerically quite difficult to treat. The problem can be simplified considerably by approximating the discrete jumps in energy suffered by an electron undergoing Compton scatterings as a continuous energy-loss process. In this case, the kinetic equation reduces to a partial differential equation. This approximation, which is accurate in the Thomson limit, also appears to be reasonably good in the Klein-Nishina regime for a wide range of target photon distributions (see, e.g., Zdziarski 1989).

Analytical solutions to the electron kinetic equation have been found for special cases e.g., when continuous or impulsive injection is considered, with the electrons cooling radiatively through synchrotron and inverse Compton scattering in the Thomson limit, as well as escaping from the system (Kardashev 1962). Although Klein-Nishina (KN) effects are well-known to have an impact on the steady-state spectra (e.g., Blumenthal 1971; Kirk et al. 1999; Dermer & Atoyan 2002; Moderski et al. 2005b), their inclusion in time-dependent models has so far necessitated a rather elaborate numerical treatment (Mastichiadis & Kirk 1997; Krawczynski et al. 2002). However, recently, a useful approximation for the treatment of the inverse Compton energy losses in an isotropic photon field, including the transition from the Thomson to the KN regime has been presented (Moderski et al. 2005a). In this paper, we use this approximation to develop a semi-analytical solution to the electron kinetic equation. The numerical treatment of the time-dependent problem is thus reduced to a single quadrature.

We use this method to discuss the temporal evolution of characteristic features in the electron distribution as a consequence of energy losses in the KN regime. These effects are of interest in the sources mentioned above, as well as in active galactic nuclei. The paper is structured in the following way: in Sect. 2, we derive our semi-analytical solution to the continuity equation that describes the temporal evolution of an electron distribution suffering synchrotron, inverse-Compton (including KN effects), and escape losses for an arbitrary, time-dependent injection spectrum. The necessary analytical calculations are summarised in Appendices A and B. Numerical results found using this method are presented in Sect. 3 and a specific application to the case of the stellar association Wd-2 is given in Sect. 4. We close the paper in Sect. 5 with a discussion of the results and comment on further refinements of the calculations.

2. Electron energy distribution

2.1. Formal solution to the kinetic equation

Assume a homogeneous source into which an unspecified acceleration process injects electrons at the rate $Q(\gamma, t)$, which subsequently cool and escape. The kinetic equation governing the evolution of the number $N(\gamma, t)$ of electrons in the source with Lorentz factors γ in the interval $\mathrm{d}\gamma$ at time t is

$$\frac{\partial N(\gamma,t)}{\partial t} = \frac{\partial}{\partial \gamma}\{\dot{\gamma}(\gamma)N(\gamma,t)\} - \nu_{\rm esc}(\gamma)N(\gamma,t) + Q(\gamma,t). \quad (1)$$

In writing Eq. (1) we have assumed that each individual electron in the source loses energy continuously, according to $\mathrm{d}\gamma/\mathrm{d}t = -\dot{\gamma}$ (note that $\dot{\gamma}$ is defined as positive) and has an energy-dependent probability $\nu_{\rm esc}(\gamma)\mathrm{d}t$ of escaping the source in a time interval $\mathrm{d}t$. The continuous-loss approximation is appropriate for synchrotron radiation and for Compton scattering in the Thomson limit, as well as for collisional losses ("ionisation losses") in a fully ionised plasma. In the case of Compton scattering in the Klein-Nishina regime, this approximation has been examined by several authors (e.g., Blumenthal 1971; Zdziarski 1989). Provided one is only interested in spectral features that appear in the transition region between the Thomson limit and the extreme Klein-Nishina limit, it appears to be justified. In addition, we assume that Eq. (1) is linear in $N(\gamma, t)$, i.e., that the the emitted radiation has no further effect on the electron distribution or on the electron injection function. This excludes situations encountered in compact sources in which feedback effects can be important (e.g., Katarzyński et al. 2006; Lightman & Zdziarski 1987; Stawarz & Kirk 2007), but is not a significant restriction for objects such as stellar clusters.

In the case discussed here where the total energy-loss rate, $\dot{\gamma}(\gamma)$, and the escape rate, $\nu_{\rm esc}(\gamma)$, are independent of time, Eq. (1) can be solved by several standard methods, e.g., by means of the Green's function for the homogeneous equation (Ginzburg & Syrovatskii 1964) or by using Laplace transforms (Melrose 1980). Following Melrose (1980), we define the quantity $\tau(\gamma', \gamma)$ as the time required for an electron to cool from a Lorentz factor of γ' to one of γ ($\leq\gamma'$),

$$\tau(\gamma',\gamma) := \int_{\gamma}^{\gamma'} \frac{\mathrm{d}\gamma''}{\dot{\gamma}(\gamma'')}; \quad (2)$$

and the quantity $\lambda(\gamma', \gamma)$, such that $1 - \exp\left[-\lambda\left(\gamma', \gamma\right)\right]$ is the probability that an electron escapes whilst cooling from γ' to γ:

$$\lambda(\gamma',\gamma) := \int_{\gamma}^{\gamma'} \mathrm{d}\gamma'' \frac{\nu_{\rm esc}(\gamma'')}{\dot{\gamma}(\gamma'')}. \quad (3)$$

This enables the solution to be written as

$$N(\gamma,t) = \frac{1}{\dot{\gamma}(\gamma)} \int_{\gamma}^{\infty} \mathrm{d}\gamma' \mathrm{e}^{-\lambda(\gamma',\gamma)} \times \left\{Q\left[\gamma', t-\tau(\gamma',\gamma)\right] H\left[t-\tau(\gamma',\gamma)\right] + N(\gamma',0)\delta\left(t-\tau(\gamma',\gamma)\right)\right\}, \quad (4)$$

where H and δ stand for the Heaviside and delta functions, respectively. On multiplying Eq. (4) by $\dot{\gamma}(\gamma)$, it is straightforward to assign a physical interpretation to each term in this solution. Thus,

- $\dot{\gamma}(\gamma)N(\gamma, t)$ is the number of particles per unit time that cool across the Lorentz factor γ,
- $\mathrm{e}^{-\lambda(\gamma',\gamma)} Q\left[\gamma', t-\tau(\gamma',\gamma)\right] H\left[t-\tau(\gamma',\gamma)\right] \mathrm{d}\gamma'$ is the rate at which particles injected with a Lorentz factor between γ' and $\gamma' + \mathrm{d}\gamma'$ arrive at time t at a Lorentz factor γ, and
- $\mathrm{e}^{-\lambda(\gamma',\gamma)} N(\gamma', 0)\delta\left(t - \tau(\gamma', \gamma)\right) \mathrm{d}\gamma'$ is the rate at which particles whose initial Lorentz factor lies between γ' and $\gamma' + \mathrm{d}\gamma'$ arrive at Lorentz factor γ at time t.

As we shall see below, the cooling rate is such that, in the limit of large Lorentz factor, synchrotron losses always dominate: $\dot{\gamma} \sim \gamma^2$ as $\gamma \to \infty$. In this case, a finite time suffices for an electron to cool down to γ from an initially arbitrarily large Lorentz factor. Defining the function $\gamma_1(t)$ as the Lorentz factor at time t of a particle whose initial energy was infinite, i.e.,

$$\tau[\infty, \gamma_1(t)] = t, \quad (5)$$

one can rewrite Eq. (4) as

$$N(\gamma,t) = \frac{1}{\dot\gamma(\gamma)}\Big\{\int_{\gamma}^{\gamma_0} \mathrm{d}\gamma' \mathrm{e}^{-\lambda(\gamma',\gamma)} \times Q\Big[\gamma', t-\tau(\gamma',\gamma)\Big] H\Big[t-\tau(\gamma',\gamma)\Big] + N(\gamma_0,0)\mathrm{e}^{-\lambda(\gamma_0,\gamma)}\Big\}, \quad \text{for } \gamma \le \gamma_1(t) \tag{6}$$

and

$$N(\gamma,t) = \frac{1}{\dot\gamma(\gamma)}\int_{\gamma}^{\infty} \mathrm{d}\gamma' \mathrm{e}^{-\lambda(\gamma',\gamma)} Q\Big[\gamma', t-\tau(\gamma',\gamma)\Big], \quad \text{for } \gamma > \gamma_1(t) \tag{7}$$

where $\gamma_0(\gamma,t)$ is defined (for $\gamma \le \gamma_1(t)$) by the relation

$$\tau(\gamma_0,\gamma) = t. \tag{8}$$

The exact functional form of Eqs. (6) and (7) is determined by the energy dependence of the radiation processes involved and the escape rate, as well as the injection function specified. As an illustration, we present the well-known case of constant injection of a power-law spectrum: $Q(\gamma,t) = Q_0\gamma^{-p}$, starting at $t = 0$ with $N(\gamma,0) = 0$, where radiative cooling is only due to synchrotron emission $\dot\gamma = b_{\rm s}\gamma^2$ and no escape term is present ($\nu_{\rm esc} = 0$). In this case $\tau(\gamma',\gamma) = (b_{\rm s}\gamma')^{-1} - (b_{\rm s}\gamma)^{-1}$ and $\lambda(\gamma',\gamma) = 0$. Equation (6) then gives (see also Melrose 1980):

$$N(\gamma,t) = \frac{Q_0\gamma^{-p}}{(p-1)b_{\rm s}\gamma}\begin{cases}[1-(1-b_{\rm s}\gamma t)^{p-1}]: & 0 \le b_{\rm s}\gamma t \le 1\\ 1: & b_{\rm s}\gamma t > 1.\end{cases} \tag{9}$$

As implied by Eq. (9) the electron spectrum steepens from γ^{-p} for $b_{\rm s}\gamma t \ll 1$ to $\gamma^{-(p+1)}$ for $b_{\rm s}\gamma t \approx 1$ with a break at $\gamma \approx 1/b_{\rm s}t = \gamma_1(t)$ that moves to lower energies as time progresses: the well-known "spectral ageing" effect.

For an injection function that is non-zero only within a range of the Lorentz factor $\gamma \in [\gamma_{\rm min},\gamma_{\rm max}]$,

$$Q = \begin{cases} Q(\gamma,t) & \text{for } \gamma_{\rm min} \le \gamma \le \gamma_{\rm max}\\ 0 & \text{otherwise,}\end{cases} \tag{10}$$

it is computationally more efficient to account for this explicitly by modifying the integration limits in Eqs. (6) and (7). Specialising to $N(\gamma,0) = 0$, one finds

$$N(\gamma,t) = \frac{1}{\dot\gamma(\gamma)}\int_{\gamma_l}^{\gamma_u} \mathrm{d}\gamma' \mathrm{e}^{-\lambda(\gamma',\gamma)} Q\Big[\gamma', t-\tau(\gamma',\gamma)\Big] H\Big[t-\tau(\gamma',\gamma)\Big], \quad \text{for } \gamma_2 \le \gamma \le \gamma_{\rm max} \tag{11}$$

with $N(\gamma,t) = 0$ for $\gamma < \gamma_2$ and $\gamma > \gamma_{\rm max}$. Here, the lower and upper integration limits are

$$(\gamma_l^{\gamma_{\rm min}<\gamma_1}, \gamma_u^{\gamma_{\rm min}<\gamma_1}) = \begin{cases}(\gamma_{\rm min},\gamma_0): & \gamma_2 < \gamma \le \gamma_{\rm min}\\ (\gamma,\gamma_0): & \gamma_{\rm min} < \gamma \le \gamma_1\\ (\gamma,\gamma_{\rm max}): & \gamma_1 < \gamma \le \gamma_{\rm max},\end{cases} \tag{12}$$

when $\gamma_{\rm min} < \gamma_1$, while

$$(\gamma_l^{\gamma_1<\gamma_{\rm min}}, \gamma_u^{\gamma_1<\gamma_{\rm min}}) = \begin{cases}(\gamma_{\rm min},\gamma_0): & \gamma_2 < \gamma \le \gamma_1\\ (\gamma_{\rm min},\gamma_{\rm max}): & \gamma_1 < \gamma \le \gamma_{\rm min}\\ (\gamma,\gamma_{\rm max}): & \gamma_{\rm min} < \gamma \le \gamma_{\rm max},\end{cases} \tag{13}$$

for $\gamma_1 < \gamma_{\rm min}$.

The value of γ_0 still fulfills Eq. (8), but γ_1 and γ_2 are now defined by

$$\tau(\gamma_{\rm max},\gamma_1) - t = 0, \tag{14}$$

$$\tau(\gamma_{\rm min},\gamma_2) - t = 0. \tag{15}$$

Equations (14) and (15) describe the two breaks, γ_1 and γ_2, introduced in the evolved spectrum due to the existence in the injection spectrum of a minimum and a maximum Lorentz factor, $\gamma_{\rm min}$ and $\gamma_{\rm max}$, respectively. Both breaks are moving to lower values as time evolves with $\gamma_2 < \gamma_1$.

As a further illustration, Appendix B presents the solution of Eq. (1) for a power-law type injection function with finite energy spectrum, where synchrotron and inverse Compton losses in the Thomson regime are present and electrons escape at a rate $\nu_{\rm esc} \propto \gamma$ (see Sect. 2.2).

2.2. Energy-loss and escape rates

In the continuous energy-loss approximation, the total energy-loss rate of a relativistic electron ($\gamma \gg 1$), averaged over an isotropic distribution and taking synchrotron cooling into account, inverse Compton scattering of the electrons on ambient photons, Coulomb losses, and Bremsstrahlung emission (in a fully ionised hydrogen gas), is given by the formula:

$$\dot\gamma_{\rm tot} = b_{\rm s}\gamma^2 + b_{\rm iC}\gamma^2 F_{\rm KN}(\gamma) + b_C(\ln\gamma + b_{\rm C}^0) + b_B\gamma(\ln\gamma + b_B^0). \tag{16}$$

The coefficients, $b_{\rm s}$, $b_{\rm iC}$, b_C, and b_B, and the constants b_C^0 and b_B^0 are given by the following relations (Ginzburg & Syrovatskii 1964):

$$b_{\rm s} = \frac{4\sigma_{\rm T}}{3m_{\rm e}c}u_{\rm B} = 1.292\times10^{-15}(B/{\rm mG})^2 \ \ {\rm s}^{-1}, \tag{17a}$$

$$b_{\rm iC} = b_{\rm s}\frac{u_0}{u_{\rm B}} = 5.204\times10^{-20}(u_0/{\rm eV\ cm}^{-3}) \ \ {\rm s}^{-1}, \tag{17b}$$

$$b_{\rm C} = \frac{2\pi e^4 n_{\rm e}}{m_{\rm e}^2c^3} = 1.491\times10^{-14}n_{\rm e} \ \ {\rm s}^{-1}, \tag{17c}$$

$$b_{\rm B} = \frac{4e^6 n_{\rm e}}{m_{\rm e}^2c^4\hbar} = 1.37\times10^{-16}n_{\rm e} \ \ {\rm s}^{-1}, \tag{17d}$$

and

$$b_{\rm C}^0 = \ln\left(\frac{m_{\rm e}^3c^4}{4e^2n_{\rm e}\hbar^2}\right) + \frac{3}{4} = -\ln n_{\rm e} + 73.4, \tag{18a}$$

$$b_{\rm B}^0 = \ln 2 - \frac{1}{3} = 0.36. \tag{18b}$$

Here, $\sigma_{\rm T}$ is the Thomson cross section, u_0, $u_{\rm B}$ are the total energy densities of the photon and magnetic fields, respectively, while c, $m_{\rm e}$, and e are the velocity of light in vacuum, the electron mass, and charge, respectively. Finally, $n_{\rm e}$ is the electron density in units of cm^{-3}. In the case of ionisation or Bremsstrahlung losses (in neutral hydrogen), the corresponding terms in Eq. (16) should be replaced by $b_{\rm C}(3\ln\gamma + 18.8)$ and $b_{\rm B}$ [ln(191) + 1/18] $\simeq$ 5.3 $b_{\rm B}$.

The escape of particles from the source may be modelled in different ways. The simplest method is to assume that the "source" is a region of relatively strong magnetic field and high

target-photon density. When particles are carried out of this region by the motion of the background plasma, they not only may leave the target fields behind, but may also undergo a sudden drop in energy due to adiabatic expansion. This scenario implies that the escape rate is independent of energy, being the reciprocal of the average time taken by a fluid element to cross the region at a given speed.

An alternative method (which, however, does not account for a possible energy loss) is to consider the particle transport as a diffusive process with the spatial diffusion coefficient $D \equiv \langle \Delta r^2 \rangle / 2t$, being either constant or a function of the energy of the particle or/and time, $D(\gamma, t)$. A common practice is to calculate the spatial diffusion coefficient in the Bohm diffusion limit, which is defined by setting the step size of the random walk of a particle equal to the Larmor radius, $r_{\rm L} = \gamma m_{\rm e} c / eB$ (for relativistic electrons). In this case, $D(\gamma) = r_{\rm L} c/3$ and the escape rate from a spherical region with radial extension R, $\nu_{\rm esc}(\gamma) = 2D(\gamma)/R^2$ is, therefore, directly proportional to the particle's energy:

$$\nu_{\rm esc}(\gamma) = b_{\rm esc}\gamma, \tag{19}$$

where $b_{\rm esc} = 2m_{\rm e}c^2/3eBR^2 = 3.6 \times 10^{-21}$ s^{-1} $(B/{\rm mG})^{-1} \cdot (R/{\rm pc})^{-2}$.

2.3. Inverse Compton scattering

The function $F_{\rm KN}(\gamma)$ in Eq. (16) takes the full Klein-Nishina cross section for Compton scattering into account and is given by the relation

$$F_{\rm KN}(\gamma) = \frac{1}{u_0} \int_0^\infty f_{\rm KN}(\gamma, \epsilon_0) u_{\epsilon_0} {\rm d}\epsilon_0, \tag{20}$$

where u_{ϵ_0} is the differential photon energy density: $u_0 = \int u_{\epsilon_0} {\rm d}\epsilon_0$ and $\epsilon_0 = h\nu/mc^2$ is the dimensionless energy of a target photon of frequency ν. The kernel, $f_{\rm KN}(\gamma, \epsilon_0)$, was first given by Jones (1965). It is important to note that this kernel, although originally derived for an isotropic field of target photons, is also valid for an anisotropic photon field, provided the average over an isotropic *electron* distribution is taken (see Kirk et al. 1999, Appendix A). A useful approximate expression in the limit $\gamma \gg \epsilon_0$ has recently been given by Moderski et al. (2005a)

$$f_{\rm KN}(\gamma, \epsilon_0) \approx (1 + 4\gamma\epsilon_0)^{-3/2},$$

for

$$\gamma\epsilon_0 \lesssim 10^4,$$

and these authors also estimate the implications of Eq. (2.3) for the functional form of $F_{\rm KN}(\gamma)$, for different photon energy distributions.

For a (possibly diluted) Planckian distribution of photon energies, the Compton energy losses for electrons are dominated by scatterings on photons with dimensionless energy $\epsilon_{\rm eff} = 2.8kT/m_{\rm e}c^2$. For $kT \ll \gamma m_{\rm e} c^2$, the function $F_{\rm KN}(\gamma)$ can therefore be approximated by treating the Planckian as a mono-energetic photon distribution (i.e., $u_{\epsilon_0} = a_0 \delta(\epsilon_0 - \epsilon_{\rm eff})$). Using this approximation and Eq. (2.3), one finds

$$F_{\rm KN}(\gamma) \approx (1 + 4\gamma\epsilon_{\rm eff})^{\beta}$$

with

$$\epsilon_{\rm eff} = 2.8kT/m_{\rm e}c^2$$

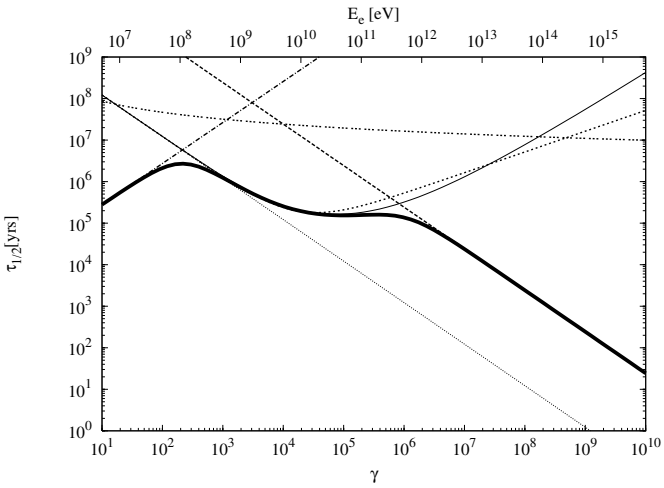

Fig. 1. The cooling time $\tau_{\rm cool} = \gamma/\dot{\gamma}$ as a function of Lorentz factor for the various energy-loss mechanisms for electrons including Coulomb scattering (dash-dotted), Bremsstrahlung (triple dotted), synchrotron (long dashed), inverse Compton (Thomson limit: dotted, approximation, see Eq. (2.3): short dashed, no approximation: thin line), and total (heavy line). The parameters are $n_{\rm e} = 1$ cm^{-3}, $u_0 = 500$ eV cm^{-3}, $T = 30\,000$ K, and $B = 10$ μG, as expected for a stellar environment with hot young stars.

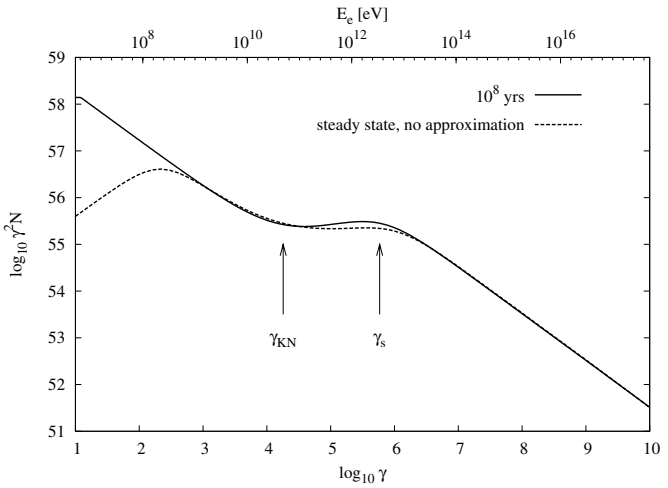

Fig. 2. The solution $N(\gamma, t = 10^8$ yrs) using the approximate cooling term of Eq. (22) in an environment identical to the one used in Fig. 1 (solid line) compared with the steady-state solution using the full expression, for $F_{\rm KN}$ and including Coulomb losses (dashed line).

and

$$\beta = -3/2.$$

For a power-law radiation field ($u_{\epsilon_0} = a_0 \epsilon_0^{-\alpha_0}$), $F_{\rm KN}(\gamma)$ can be written in the same general form as in Eq. (2.3), provided the values of the parameters $\epsilon_{\rm eff}$ and β are suitably chosen. For $\alpha_0 < -0.5$ and $\alpha_0 > 1$, inverse Compton losses in the KN limit are dominated by scatterings on photons with the highest ($\approx\epsilon_{0,\rm max}$) and the lowest ($\approx\epsilon_{0,\rm min}$) photon energies available, respectively. One may therefore write $\epsilon_{\rm eff} = \epsilon_{0,\rm max}$ for $\alpha_0 < -0.5$ and $\epsilon_{\rm eff} = \epsilon_{0,\rm min}$ for $\alpha_0 > 1$, with $\beta = -3/2$ in each case.

In the intermediate case of $-0.5 < \alpha_0 < 1$, the relevant photon energy range for scattering is broader ($\approx 1/4\gamma$) and one may instead use the so-called "Thomson edge" or "KN cut-off" approximation. In this range $F_{\rm KN}(\gamma)$ is still given by Eq. (2.3) with $\epsilon_{\rm eff} = \epsilon_{0,\rm max}$ and $\beta = \alpha_0 - 1$, provided $\epsilon_{0,\rm min}/\epsilon_{0,\rm max} \ll 1$. Table 1

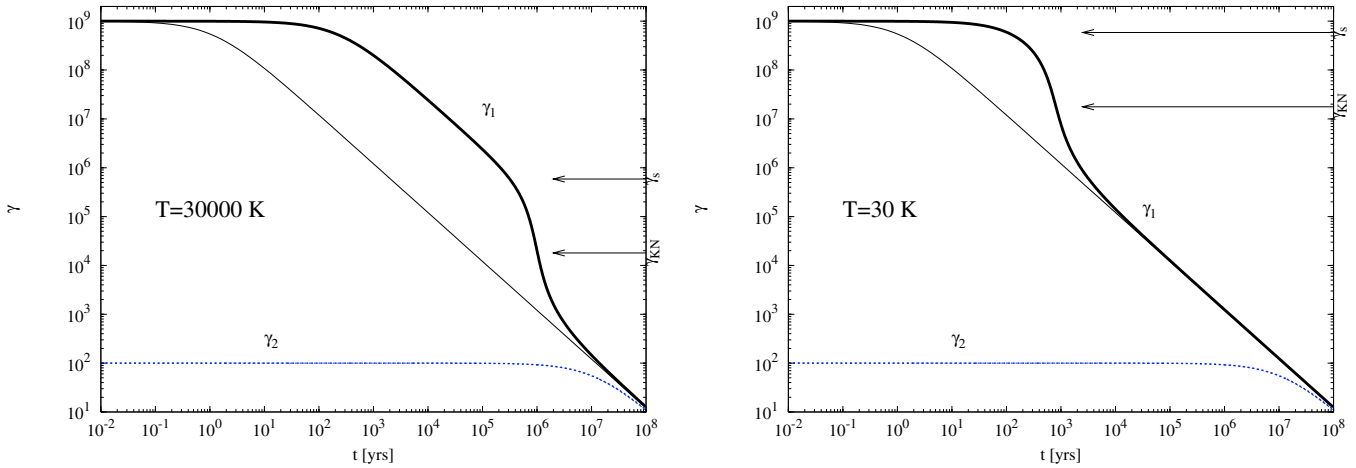

Fig. 3. The quantities γ_1 and γ_2 defined in Eqs. (14) and (15) as functions of time for magnetic fields and target photon fields of the same energy density but for two different photon temperatures: $T = 30\,000$ K (*left panel*) and $T = 30$ K (*right panel*). In both panels, γ_s (transition from synchrotron to KN cooling) and γ_{KN} (transition from KN to Thomson) are indicated by horizontal arrows. For comparison, the thin lines indicate the evolution of γ_1 and γ_2 in the Thomson limit (for γ_2, the cooling proceeds at all times in the Thomson regime, since γ_{min} is chosen to be 100; therefore, the two curves are superposed).

summarises the values of the parameters ϵ_{eff} and β for the case of a black-body photon targets, as well as for power-law target photon fields.

The cooling timescale for electrons $\tau_{cool}(\gamma) = \gamma/\dot{\gamma}$ for the various energy-loss mechanisms, assuming an environment where inverse Compton cooling in the Klein-Nishina limit is important, is shown in Fig. 1. The parameters used are $n_e = 1$ cm^{-3}, $u_0 = 500$ eV cm^{-3}, $T = 30\,000$ K, and $B = 10$ μG, as expected in an environment dominated by hot and young stars that provide a relatively high-temperature target-photon field. The cooling time for Coulomb scattering and Bremsstrahlung losses is calculated assuming a fully ionised gas. This is a self-consistent assumption taking the high-temperature and energy density of the ambient photon field into account, which is sufficient to ionise neutral hydrogen. The cooling time is dominated by different mechanisms in different energy ranges. At the lowest energies, Coulomb scattering ("ionisation loss") is the fastest energy loss mechanism, whereas inverse Compton scattering in the Thomson regime takes over above approximately 100 MeV. For electron energies above a few GeV, the inverse Compton scattering becomes less efficient because of the drop in the cross section. At energies higher than 1 TeV, inverse Compton scattering is less efficient than synchrotron radiation, which remains the dominant mechanism at higher energies. Although these transition energies depend on the choice of the parameters (u_0, n_e, T, and B), the qualitative picture remains the same. It is interesting to compare the approximation for $F_{KN}(\gamma)$ with the "exact" calculation shown in Fig. 1 (using the expression for $f_{KN}(\gamma, \epsilon_0)$ given by Moderski et al. 2005a). The approximation slightly overpredicts τ_{cool}, but is fairly accurate up to very high energies (~10% at $E \simeq 10^{14}$ eV, corresponding to $\gamma\epsilon_{eff} \simeq 10^4$). However, as one can readily deduce from Fig. 1, the approximation for $F_{KN}(\gamma)$ becomes inaccurate only in the regime where synchrotron losses are likely to dominate. Even in binary systems, where the radiation field density can be substantially higher than the value assumed in Fig. 1, the ratio of u_0/u_B is unlikely to be higher than $O(1000)$ and, therefore, electrons with $\gamma\epsilon_{eff} \gtrsim 10^4$ cool predominantly through synchrotron radiation.

Table 1. The values of the parameters β and ϵ_{eff} (see Eq. (2.3)) for two different photon energy distributions.

Photon distribution	β	ϵ_{eff}
Planck, temperature T	$-3/2$	$2.8kT/m_ec^2$
power law, $\alpha_0 < -0.5$	$-3/2$	$\epsilon_{0,max}$
power law, $-0.5 < \alpha_0 < 1$	$\alpha_0 - 1$	$\epsilon_{0,max}$
power law, $\alpha_0 > 1$	$-3/2$	$\epsilon_{0,min}$

2.4. Time-dependent solutions for the particle distribution

For astrophysical environments with dilute plasma and fields of high energy density, the most relevant energy-loss mechanisms for high-energy electrons are synchrotron and inverse Compton radiation. Therefore, one may safely discard in this case the last two terms in Eq. (16), which then becomes

$$\dot{\gamma} = b_s\gamma^2\left[1 + b_{is}F_{KN}(\gamma)\right], \tag{21}$$

where $b_{is} \equiv b_{iC}/b_s = u_0/u_B$ denotes the ratio of the photon field total energy density to the magnetic field energy density. Using Eqs. (2.3) and (21), we may write this in the general form:

$$\dot{\gamma} = b_s\gamma^2\left[1 + b_{is}\left(1 + 4\gamma\epsilon_{eff}\right)^{\beta}\right], \tag{22}$$

where β and ϵ_{eff} are chosen from Table 1 for the appropriate target photon field. Taking Eqs. (19) and (22) into account, the functions describing cooling time and escape probability given in Eq. (3) can be expressed as

$$\tau(\gamma', \gamma) = \int_{\gamma}^{\gamma'} \frac{d\gamma''}{b_s\gamma''^2\left[1 + b_{is}\left(1 + 4\gamma''\epsilon_{eff}\right)^{\beta}\right]} \tag{23}$$

$$\lambda(\gamma', \gamma) = \int_{\gamma}^{\gamma'} \frac{b_{es}d\gamma''}{\gamma''\left[1 + b_{is}\left(1 + 4\gamma''\epsilon_{eff}\right)^{\beta}\right]} \tag{24}$$

where the notation $b_{es} \equiv b_{esc}/b_s$ has been used. Note that for $\gamma' \to \infty$, $\tau(\gamma', \gamma)$ remains finite, whereas $\lambda(\gamma', \gamma)$ diverges. Physically, this is because the synchrotron cooling rate, which goes as γ^2 dominates at high Lorentz factors, so that the time taken to cool to γ from an arbitrarily large γ' is finite. However,

if the mean free path of the electrons increases in proportion to γ, as in the case of Bohm diffusion, the probability of escape during this finite cooling time tends to unity as $\gamma' \to \infty$.

In Appendix A, we give the analytical form of the functions $\tau(\gamma', \gamma)$ and $\lambda(\gamma', \gamma)$ assuming that $\nu_{\rm esc}(\gamma) \propto \gamma$ (see Eq. 19). For a power-law type photon energy spectrum with spectral index $-0.5 < \alpha_0 < 1$, these functions are given only in closed form for the special cases $\alpha_0 = 0$ and $\alpha_0 = 1/2$, although a numerical evaluation is straightforward using Eqs. (A.1) and (A.2). The analytical expressions have the advantage that the solution of Eq. (1) is reduced to the single quadrature given in Eqs. (6) and (7) or (11).

In the Thomson limit for Compton scattering $F_{\rm KN} \simeq 1$. Therefore, assuming $\nu_{\rm esc} = b_{\rm esc}\gamma$, one has $\beta = 0$ in Eqs. (23) and (24), and the functions $\tau(\gamma', \gamma)$ and $\lambda(\gamma', \gamma)$ can be written down explicitly:

$$\dot{\gamma} = (b_{\rm s} + b_{\rm iC})\gamma^2 \equiv b\gamma^2 \tag{25}$$

$$\tau(\gamma', \gamma) = \frac{1}{b}\left(\frac{1}{\gamma} - \frac{1}{\gamma'}\right) \tag{26}$$

and

$$\lambda(\gamma', \gamma) = \frac{b_{\rm esc}}{b} \ln\left(\frac{\gamma'}{\gamma}\right). \tag{27}$$

The solution of Eq. (1) follows from Eqs. (6) and (7). For $\gamma < \gamma_1(t) = 1/(bt)$,

$$N(\gamma, t) = \frac{1}{b\gamma^{(2b-b_{\rm esc})/b}}\left[\int_{\gamma}^{\gamma_0} {\rm d}\gamma' \gamma'^{-b_{\rm esc}/b} \times Q\left(\gamma', t - \frac{1}{b\gamma} + \frac{1}{b\gamma'}\right) H\left(t - \frac{1}{b\gamma} + \frac{1}{b\gamma'}\right)\right] + \frac{1}{b\gamma^2}\left(\frac{\gamma}{\gamma_0}\right)^{b_{\rm esc}/b} N(\gamma_0, 0), \tag{28}$$

where $\gamma_0 = \gamma/(1 - bt\gamma)$ and, for $\gamma > 1/(bt)$,

$$N(\gamma, t) = \frac{1}{b\gamma^{(2b-b_{\rm esc})/b}} \int_{\gamma}^{\infty} {\rm d}\gamma' \gamma'^{-b_{\rm esc}/b} Q\left(\gamma', t - \frac{1}{b\gamma} + \frac{1}{b\gamma'}\right). \tag{29}$$

The solution for a continuous power-law injection with a finite energy spectrum is given in Appendix B.

In the case where the escape rate does not depend on the particle energy, $\lambda(\gamma', \gamma) = \tau(\gamma', \gamma)/t_{\rm esc}$, where $t_{\rm esc} = 1/\nu_{\rm esc} =$ const. Then, in the Thomson limit of Compton scattering, $\tau(\gamma'\gamma)$ is given, as before, by Eq. (26), and from Eq. (6) one finds

$$N(\gamma, t) = \frac{1}{b\gamma^2} {\rm e}^{-t_{\rm cool}/t_{\rm esc}} \left\{\int_{\gamma}^{\gamma_0} {\rm d}\gamma' {\rm e}^{1/b\gamma' t_{\rm esc}} \times Q\left[\gamma', t - (b\gamma)^{-1} + (b\gamma')^{-1}\right] H\left[t - (b\gamma)^{-1} + (b\gamma')^{-1}\right]\right\} + \frac{1}{b\gamma^2} {\rm e}^{-t_{\rm cool}/t_{\rm esc}} N(\gamma_0, 0) {\rm e}^{1/bt_{\rm esc}\gamma_0}, \tag{30}$$

for $\gamma > 1/(bt)$, and for $\gamma < 1/(bt)$:

$$N(\gamma, t) = \frac{1}{b\gamma^2} {\rm e}^{-t_{\rm cool}/t_{\rm esc}} \times \int_{\gamma}^{\infty} {\rm d}\gamma' {\rm e}^{1/b\gamma' t_{\rm esc}} Q\left[\gamma', t - (b\gamma)^{-1} + (b\gamma')^{-1}\right], \tag{31}$$

where the cooling time $t_{\rm cool}(\gamma) := \tau(\infty, \gamma) = 1/b\gamma$ is the time taken for an electron to cool from infinite Lorentz factor to Lorentz factor γ. For $N(\gamma, 0) = 0$, with a constant mono-energetic injection spectrum, $Q(\gamma, t) = Q_0 H(t)\delta(\gamma - \gamma_i)$, and for $\gamma_i > \gamma > \gamma_i/(1 + bt\gamma_i)$, Eq. (30) yields a steady-state solution:

$$N(\gamma, t) = \frac{Q_0}{b\gamma^2} {\rm e}^{-t_{\rm cool}/t_{\rm esc} + 1/\gamma_i t_{\rm esc}}. \tag{32}$$

This solution displays a cut-off towards lower Lorentz factors at $t_{\rm cool} = t_{\rm esc}$ as has been pointed out by Kardashev (1962).

3. Numerical results

3.1. Comparison with the steady-state solution

Ignoring escape losses, Eq. (1) in the steady-state limit, $\partial N/\partial t \to 0$ becomes

$$\frac{\rm d}{{\rm d}\gamma}\{\dot{\gamma} N(\gamma)\} + Q(\gamma) = 0, \tag{33}$$

which is easily integrated to give

$$N(\gamma) = -\dot{\gamma}^{-1} \int_{\gamma}^{\infty} Q(\gamma') {\rm d}\gamma'. \tag{34}$$

In this case it is straightforward to incorporate the general term for $\dot{\gamma}$ given by Eq. (16). In Fig. 2, we compare this solution with the time-dependent solution obtained by using Eqs. (6) and (7) with the approximate cooling term given in Eq. (22). We take $t = 10^8$ years, which is sufficiently large to allow a steady state to be achieved, and assume no particles are present initially, $N(\gamma, 0) = 0$. In this figure, escape is neglected, $b_{\rm es} = 0$, and the ratio of the energy density of the photon field to that of the magnetic field is $b_{\rm is} = 200$. The remaining parameters are the same as in Fig. 1 Note that here and in the following, we restrict our calculations to the case of a thermal distribution of target photons. The qualitative picture is similar to the case of a photon field following a power law.

For $\gamma \lesssim 100$, Coulomb losses harden the spectrum to $p - 1 = 1$. Since the time-dependent solution is based upon a "simplified" energy-loss term given in Eq. (21) neglecting the Coulomb energy losses, the two solutions deviate in this range. Between $\gamma \simeq 300$ and $\gamma \simeq \gamma_{\rm KN} = (4\ \epsilon_0)^{-1} \approx 18\,000(T/30\,000\ {\rm K})^{-1}$, electrons cool predominantly via inverse Compton scattering in the Thomson limit. For values of $\gamma > \gamma_{\rm KN}$, the drop in the inverse Compton scattering cross section in the Klein-Nishina regime leads to a spectral hardening until synchrotron losses become dominant for $\gamma \gtrsim \gamma_{\rm s} = (b_{\rm is}^{2/3} - 1)/(4\epsilon_0) \approx 6 \times 10^5 (b_{\rm is}/200)^{2/3}(T/30\,000\ {\rm K})^{-1}$. The positions of $\gamma_{\rm KN}$ and $\gamma_{\rm s}$ are indicated in Fig. 2. The slight deviation observed for $\gamma_{\rm KN} \lesssim \gamma \lesssim \gamma_{\rm s}$ is the result of the approximation used for $F_{\rm KN}$ given in Eq. (2.3). From Fig. 2, it is obvious that (a) the approximation used to take the energy dependence of the inverse Compton scattering cross section into account follows the exact calculation quite well and (b) neglecting Coulomb losses mainly affects the low-energy part of the spectrum.

3.2. Temporal evolution

The temporal evolution of $N(\gamma, t)$ for an arbitrary injection function $Q(\gamma, t)$ can now be calculated. In the following we investigate the impact of the relevant parameters ($b_{\rm s}, b_{\rm is}, b_{\rm es}, T$). To

demonstrate the effect of KN cooling on the temporal evolution, we plot the evolution of γ_1 and γ_2 in Fig. 3 as a function of time for two different temperatures ($T = 30\,000$ K and $T = 30$ K), which are representative of an environment dominated by either hot stars or by re-processed emission from warm dust. For comparison, the evolution of γ_1 and γ_2 in the Thomson limit is depicted by thin lines. In both cases, the parameters have been chosen similar to the ones used above ($B = 10\ \mu$G, $u_0 = 500$ eV cm^{-3} corresponding to $b_{\rm is} = 200$, $b_{\rm es} = 0$) with $\gamma_{\rm min} = 100$ and $\gamma_{\rm max} = 10^9$. The evolution of γ_2 is dominated by slow cooling in the Thomson limit, and therefore, the two lines are identical. For the high-temperature environment (Fig. 3a), γ_1 cools via synchrotron radiation until roughly 1 Myr, when the energy losses in the KN limit take over. Within a few hundred thousand years, the transition to Thomson-limit cooling takes place when $\gamma_1 < \gamma_{\rm KN}$. Qualitatively, the evolution of γ_1 for a cooler photon field proceeds in a similar way (Fig. 3b). It is, however, important to note that the respective transitions occur much earlier. Whereas for $T = 30\,000$ K, synchrotron cooling prevails for about 1 Myr, for $T = 30$ K, Compton cooling in the KN regime is reached within a few hundred years.

The effect on the temporal evolution of a particle distribution that is partially cooling via inverse Compton radiation in the KN limit is shown in Fig. 4. Here, we have assumed a continuous power-law electron injection with $p = 2$ between $\gamma_{\rm min} = 10^2$ and $\gamma_{\rm max} = 10^9$, neglected escape losses ($b_{\rm es} = 0$), and included the environmental parameters described above. The solutions $N(\gamma, t)$ for $t = 10^5$, 8×10^5, and 2×10^6 years, weighted with γ^2 so that the injected spectrum appears constant, are compared with solutions found by using expressions for the cooling valid in the Thomson limit (see Appendix B), which are depicted as thin lines.

The solutions for $t = 10^5$ yrs (see also Fig. 3a) correspond to the case $\gamma_1 > \gamma_{\rm s}$ (the position of γ_1 marked in Fig. 4). The solution taking KN effects into account shows a break such that $N \propto \gamma^{-(p+1)}$ for $\gamma > \gamma_1$, while for smaller $\gamma_{\rm KN} < \gamma < \gamma_{\rm s}$, a slight deviation from the $p = 2$ injection power law can be observed to mark the onset of rapid energy loss in the KN regime. In the solution obtained in the Thomson limit, the break occurs at a lower value of γ_1 (see also Fig. 3a), which marks the transition from the uncooled part of the spectrum to the part that has already suffered from cooling. At the solution at a later time ($t = 8 \times 10^5$ yrs) when $\gamma_{\rm KN} < \gamma_1 < \gamma_{\rm s}$, the flattened spectral shape presented earlier in the steady-state solution (see Fig. 2) has already developed fully as a consequence of the large $\dot{\gamma}$ in the KN regime. The solution obtained in the Thomson limit and the one obtained taking KN effects into account agree with each other for $\gamma < \gamma_{\rm KN}$, which marks the transition to cooling in the Thomson limit. Finally, for $t = 2 \times 10^6$ yrs, $\gamma_1 < \gamma_{\rm KN}$, and the further temporal evolution is described in the Thomson limit well.

In the next example, we consider a higher value of $\gamma_{\rm min} = 10^4$ while keeping the same values for all other parameters as in the examples above. Figure 5 shows $N(\gamma, t)$ for three different times: $t = 10$, 10^4, and 10^7 years. The shape of the spectrum mainly evolves, as expected, due to synchrotron cooling for $t \lesssim 10^6$ years. At later times (e.g., $t = 10^7$ yrs), the spectrum shows a smooth transition between $p = 2$ and $p + 1 = 3$ at $\gamma \approx \gamma_{\rm s}$. For lower values of γ, the spectrum remains almost flat, showing a slight peak at the position of $\gamma_{\rm min}$. The overall shape of this evolved spectrum could, in principle, mimic the case of an uncooled spectrum up to TeV energies (depending on the value of $b_{\rm is}$) with a softening at $\gamma \approx \gamma_{\rm s}$ resembling a much younger source. Remarkably, for $p = 2$, the effect of cooling in KN is almost hidden when $\gamma_{\rm min} \approx \gamma_{\rm KN}$. For higher values of $b_{\rm is}$, a hard particle spectrum can be retained up to even higher values of γ than those shown here (see also next example).

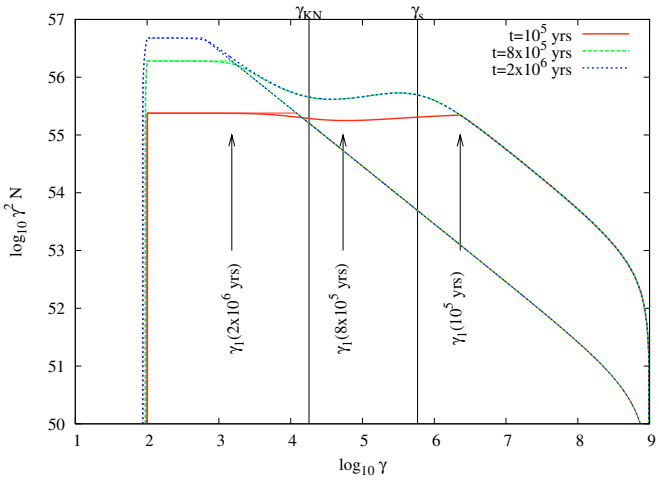

Fig. 4. The solution $N(\gamma, t)$ obtained by including the effects of KN cooling (thick lines) and in the Thomson limit (see Appendix C) for three different times chosen such that $\gamma_1 > \gamma_{\rm s}$ ($t = 10^5$ yrs), $\gamma_{\rm KN} < \gamma_1 < \gamma_{\rm s}$ ($t = 8 \times 10^5$ yrs), and $\gamma_1 < \gamma_{\rm KN}$ ($t = 2 \times 10^6$ yrs). The parameters used are identical to the ones used e.g. in Fig. 3a. The positions of γ_1 at different times, as well as of $\gamma_{\rm KN}$ and $\gamma_{\rm s}$, are indicated by arrows and vertical lines, respectively.

Changing the ratio of the photon and magnetic field energy densities ($b_{\rm is}$) at a fixed photon temperature influences the location of the transition between inverse Compton and synchrotron cooling. In Fig. 6, the effect of varying $b_{\rm is}$ from values of 100 up to 10^4 is demonstrated. Increasing $b_{\rm is}$ leads to more rapid cooling and a more pronounced spectral hardening as a result of inverse Compton cooling in the KN limit.

Finally, we consider the effect of particle escape via diffusive particle transport leaving a sphere with radius R. In Fig. 7, the solution $N(\gamma, t)$ is shown for values of $b_{\rm es} = 0.1$, 100, and 1000 at $t = 10^6$ yrs. For comparison, the solution of Appendix B in the Thomson limit is also shown. All other parameters are the same as in the previous example. As expected, the effect of escape losses leads to a reduction in the total particle number. Escape losses are negligible for $b_{\rm es} = 0.1$, whereas for $b_{\rm es} = 100$ and $b_{\rm es} = 1000$, escape losses modify the solution considerably in comparison to the case of small $b_{\rm es}$. The solution taking KN effects into account shows a stronger relative suppression of particle numbers for $\gamma > \gamma_{\rm S}$ than in the Thomson limit. This is a consequence of radiative cooling being dominated by synchrotron losses for $\gamma > \gamma_{\rm S}$ in the KN case which implies that escape losses are relatively more important ($\lambda(\gamma', \gamma) \sim b_{\rm esc}/b_s$) than in the Thomson limit, where $\lambda(\gamma', \gamma) \sim b_{\rm esc}/b$ with $b = b_{\rm s} + b_{\rm iC}$. In general, when escape losses are important, the spectral features characteristic of cooling in the KN limit are suppressed, and the solution resembles what is found in the Thomson limit. Asymptotically, for very large $b_{\rm es} \gg b$, radiative cooling is negligible and the two solutions converge.

4. Application to a stellar association: Westerlund 2

The discovery of VHE gamma-ray emission from young stellar associations like Westerlund 2 (Wd-2), Cyg OB2, and Berkeley 87 provides first clear evidence that particle acceleration can occur in these systems. While the origin of the emission and the nature of the accelerated particles is not clear, it has been suggested

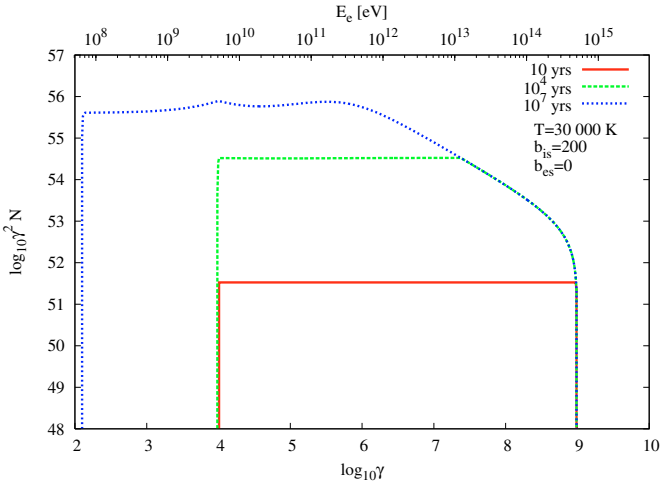

Fig. 5. Temporal evolution of an electron distribution injected with $p = 2$ between $\gamma_{\rm min} = 10^4$ and $\gamma_{\rm max} = 10^9$ in a hot ($T = 30\,000$ K) photon field. The evolution is shown for three distinct times: $t = 10$, 10^4, and 10^7 years. The energy density of the photon field is 200 times that of the magnetic field ($b_{\rm is} = 200$), and escape losses are neglected ($b_{\rm es} = 0$).

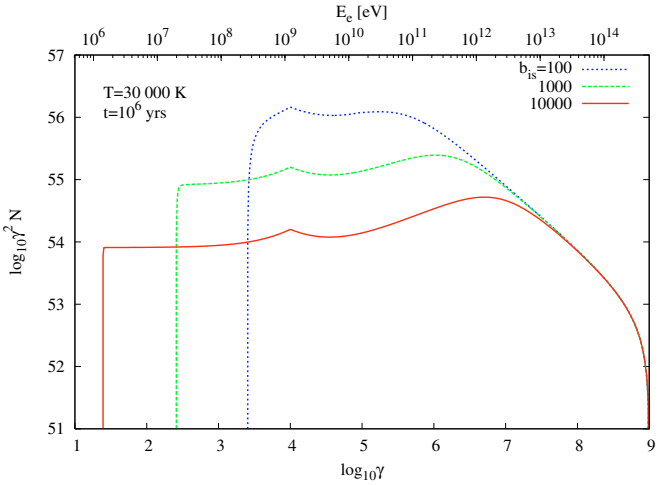

Fig. 6. The effect of varying $b_{\rm is} = 100, 1000, 10^4$ demonstrated for a similar set of parameters as described in Fig. 5 and a fixed time ($t = 10^6$ yrs).

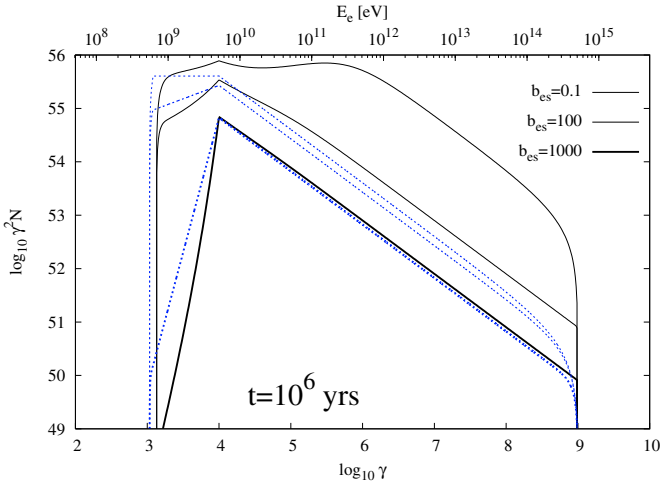

Fig. 7. The effect of escape losses is demonstrated for three different values of $b_{\rm es} = 0.1, 100, 1000$ (thin, medium, and heavy lines). The time has been fixed to 1 Myr. The injection rate, as well as the other parameters, are identical to the cases discussed in the previous figures. The solid lines are obtained taking KN effects into account, while for comparison the analytical solution for the Thomson limit is shown with dashed lines.

that gamma rays from stellar associations could be the decay product of neutral mesons in inelastic scattering of nuclei with the ambient medium (Torres et al. 2004; Bednarek 2007) or could be due to the excitation of giant resonances of nuclei by Doppler boosted UV photons (Anchordoqui et al. 2007b). Here, we calculate the broad-band spectral energy distribution of Wd-2 at different stages of its evolution. The distance to this system is not very well-constrained (Churchwell et al. 2004). A recent estimate places Wd-2 at 2.8 kpc, with an age of 2.0±0.3 Myr and a total mass of $10^4\,M_\odot$ (Ascenso et al. 2007). While this distance estimate is based mainly on near infra-red photometry and colours, the spectroscopic investigation of the cluster and the light curve of the binary system WR 20a has provided a larger distance estimate of 8.0 ± 1.4 kpc (Rauw et al. 2007). Another recent distance estimate is based upon the possible association of RCW 49 with a giant molecular cloud with a mass of $7.5 \times 10^5\,M_\odot$ at a kinematic distance of 6.0 ± 1.0 kpc (Dame 2007). For our calculations, we adopt a distance of $D = 2.8$ kpc and note that the larger distance would affect the total energetics, requiring a higher injection rate.

The angular extension, (0.18±0.02)°, of the VHE gamma-ray emission region (Aharonian et al. 2007) implies a radial extension of 8.8 pc · (D/2.8 kpc). The total luminosity of the member stars of O-type has been estimated to be $L_{\rm bol} \approx 3 \times 10^{40}$ erg s^{-1} (Rauw et al. 2007). However, it is well known that the number of UV photons emitted by the early cluster member stars is not sufficient to power the HII region RCW 49 in which Wd-2 is embedded. Based upon the estimates of Rauw et al. (2007), only ≈20% of the UV photons required to power RCW 49 can be attributed to known O stars; therefore, the assumed luminosity of the early type stars is certainly a lower limit and the total luminosity could in fact reach values beyond 10^{41} erg s^{-1}. It is noteworthy that the population of later type stars shows a rather flat projected spatial distribution even beyond a distance of 4 pc (Ascenso et al. 2007), which would lead to a higher average energy density of the photon field. In addition to the stellar photons, re-processed emission from the dust present in Wd-2, and its surrounding will provide a contribution to the seed photon field for inverse Compton scattering, which is not included here and is left for a more detailed modelling.

Taking into account just the total power emitted by the early type stars in the cluster, the average energy density of the hot photon field at a distance R corresponding to the extension of the VHE gamma-ray source can be estimated as

$$u_0 = 13\,500\,\frac{\rm eV}{\rm cm^3}\left(\frac{L_{\rm bol}}{3\times10^{40}\ {\rm ergs\ s^{-1}}}\right)\left(\frac{R}{\rm pc}\right)^{-2}. \quad (35)$$

Based upon the extension of the VHE source of 8.8 pc, $u_0 = 174$ eV cm^{-3}. However, given the presence of additional (diffuse) UV photons implied by the ionisation state of RCW 49, we choose $u_0 = 500$ eV cm^{-3} as the average energy density and a temperature of $T = 30\,000$ K to characterise the target photon field. The magnetic field is set to 10 μG, placing it in approximate equipartition to the thermal energy density of the gas, assuming a source radius of 8.8 pc. The injection rate $Q(\gamma)$ is assumed to be constant in time with a total power of 7×10^{35} ergs s^{-1} following a power law with $p = 2$ between $\gamma_{\rm min} = 10^4$ and $\gamma_{\rm max} = 3 \times 10^8$. The required injection power can be compared, for example, with the total power injected by

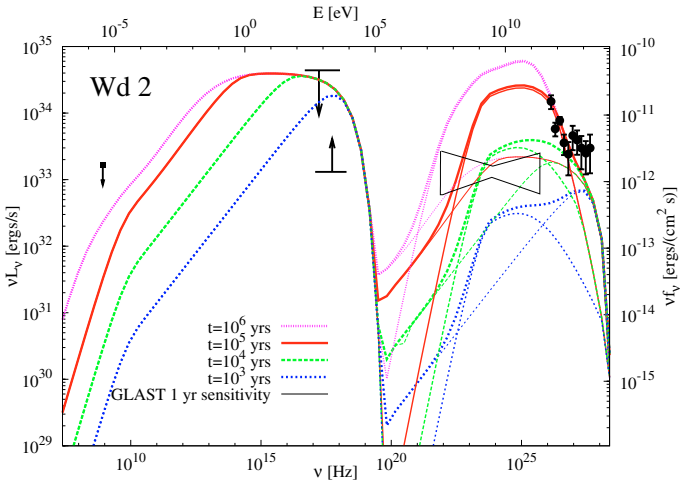

Fig. 8. Broad-band spectral energy distribution of Westerlund 2 (Wd 2) and multi-wavelength measurements (for further details see the text). For the inverse Compton emission, the heavy line indicates the sum of the emissivity from the stellar light (medium curve) allowing for KN effects as well as from the cosmic microwave background (thin curve).

the stellar winds driven by the early type stars (mainly the Wolf-Rayet stars WR 20a&b) present in Wd-2, which has been estimated as 5×10^{37} erg s^{-1} (Rauw et al. 2007). If the emitting electrons are accelerated by these stellar winds, they must take roughly 1% of the kinetic power of the bulk flow.

In hadronic scenarios, on the other hand, the required efficiency is generally much greater, because of the relatively long cooling times involved. For example, inelastic proton-proton scattering producing π^0 operates on a timescale of $t(pp \rightarrow \pi^0 + \ldots) \approx 1.5 \times 10^8 n_1^{-1}$ yrs ($n = n_1$ cm^{-3} denotes the ambient medium density), which is larger than the age of the accelerator, assuming this is limited to the maximum time that massive stars drive strong and fast stellar winds in their Wolf-Rayet phase (this lasts approximately, $t_{\rm WR} \approx 5 \times 10^5$ yrs, see also below). This implies that, under most conditions, the efficiency required in hadronic models is close or larger than unity. A similar conclusion can be drawn for the case of gamma-ray production through photo-excitation of heavy nuclei, where the efficiency of acceleration of exclusively iron nuclei has to reach values in excess of 8% (Anchordoqui et al. 2007a).

The electron distribution $N(\gamma, t)$ is computed for four different times $t = 10^3$, 10^4, 10^5, and 10^6 years. The synchrotron and inverse Compton emissivities are calculated following the approach described in Appendix C, and the resulting broad band spectral energy distribution (SED) is presented in Fig. 8. In addition to the UV photons from the early type stars, CMB photons are, of course, also present with an energy density $u_{\rm CMB} = 0.26$ eV cm^{-3}. Although the energy loss due to inverse Compton scattering on these photons is negligible, they are nevertheless quite important for the total hard gamma-ray emission. This is because for sufficiently large γ the inverse Compton scattering off UV photons is strongly suppressed, leading to emissivities that are smaller than the contribution from scattering with CMB photons. We therefore include the CMB photon field in the inverse Compton emissivity calculation and show in Fig. 8 the total inverse Compton emission as well as the contribution from UV photons and from CMB photons. It is interesting to note how the inverse Compton emission from the CMB photons dominates for young sources. With increasing age, the UV-related component at about 1 TeV increases steadily until, after $\approx 10^6$ years – roughly the age of this stellar cluster – it exceeds the CMB-related contribution. This effect is due to the accumulation of electrons of Lorentz factor ($\gamma \approx 10^6$) within the source (see Fig. 5).

The model SED is compared in Fig. 8 with VHE measurements (Aharonian et al. 2007) and with X-ray measurements by Townsley et al. (2005) taken with Chandra (indicated as a lower limit) and earlier measurements taken with the Einstein X-ray telescope (Goldwurm et al. 1987; indicated as an upper limit). While the limited field of view of the Chandra observations may underestimate the total extended X-ray emission, the Einstein observations may overestimate the diffuse flux, because of the limited spatial resolution that does not allow the subtraction of the point sources present. In this figure we also show the total integrated radio flux of 210 Jy at 843 MHz. This we consider as an upper limit that should not be exceeded by the non-thermal radio flux produced by the energetic electrons (Whiteoak & Uchida 1997). Overall, the model SED is in good agreement with the observations. The VHE energy spectrum is reproduced well for $t > 10^5$ years, and the constraints from X-ray and radio measurements are not violated. It is interesting to note that, for stars with $M > 25\,M_\odot$, the Wolf-Rayet phase is expected to last up to roughly $t_{\rm WR} \approx 5 \times 10^5$ years (Maeder & Meynet 1987), which is consistent with the injection time required to match the data in this model. In contrast, an age of $t > 10^5$ yrs would be too long for acceleration in a supernova remnant, a hypothesis that also has to contend with the fact that, so far, no indication for the presence of a supernova remnant associated with Wd-2 has been reported.

The predicted X-ray flux is quite close to the upper bound imposed by the Einstein measurements. However, it should be noted that this prediction is sensitive to the energy density in the target photon field – a factor of 2 increase in the energy density in the seed-photon field (either from the late type stars and/or emission from dust) reduces the required injection power and, consequently, the predicted X-ray flux is also reduced by a factor of 2. We also indicate the one year flux sensitivity of the upcoming GLAST gamma-ray mission[1] in Fig. 8. Our calculations predict that GLAST should detect the source easily. The combined energy spectrum of GLAST and HESS would provide a broad band energy spectrum that in turn might allow one to infer, for example, the age of the source in the model scenario suggested here.

5. Conclusions

We have presented a method for computing the time-dependent electron distribution in the continuous energy loss limit for an arbitrary source function, under the assumptions of

- an isotropic electron distribution;
- negligible ionisation and Bremsstrahlung losses;
- time-independent energy losses by synchrotron radiation in a homogeneous magnetic field and
- by inverse Compton scattering off a spatially homogeneous mono-energetic or power-law energy distribution of target photons;
- an escape probability proportional to the particle energy, as expected for diffusion in the Bohm limit.

The key innovation of the model is that it utilises a simplified expression introduced by Moderski et al. (2005b) for the inverse

[1] Taken from `www-glast.slac.stan.edu`, official GLAST homepage.

Compton scattering rate (including KN-effects) to construct explicit analytic expressions (see Appendix A) for the integrated cooling time ($\tau(\gamma',\gamma)$, Eq. (2)) and the integrated escape function ($\lambda(\gamma',\gamma)$, Eq. (3)). This enables the electron distribution to be computed in a single quadrature.

The extension of this approach to different energy dependencies of the escape probability would be relatively straightforward. However, the treatment of multiple and/or time-dependent target photon fields would probably require numerical evaluation of the functions τ and λ.

Based upon the method presented here, we have provided an in-depth discussion of the properties of cooling electron distributions and have identified features characteristic of cooling by inverse Compton scattering:

1. The effect of "spectral ageing" observed in the Thomson limit is strongly modified. While a well-defined spectral break γ_1 changes position with time in the Thomson limit (cooling break), this spectral break is no longer evident for $\gamma_1 < \gamma_s$, when KN effects are taken into account (see Fig. 4).
2. For $\gamma_{KN} < \gamma < \gamma_s$, a spectral hardening is observed as a result of cooling in the KN regime (see Figs. 2 and 4).
3. When choosing $\gamma_{min} \approx \gamma_{KN}$, the evolved spectrum shows a smooth transition at γ_s resembling a cooling break. However, this transition is stationary in time and may be mistakenly interpreted as a cooling break (see e.g. Figs. 5, 6).
4. The effect of particle escape modifies the observed energy spectra more strong for $\gamma > \gamma_s$ than for lower values of γ, which can lead to energy spectra resembling the ones obtained in the Thomson limit more (see Fig. 7).

We have illustrated our technique by applying it to high-energy observations of the open stellar cluster Westerlund 2, and calculating the broad band emission spectrum. Comparing our results with the available observations, we identified a consistent set of parameters: $b_{is} = 200$, $B = 10\,\mu$G, $T = 30\,000$ K, total injected power in electrons 7×10^{35} erg s^{-1}, distance = 2.8 kpc, $R = 8.8$ pc, $\gamma_{min} = 10^4$, $\gamma_{max} = 3 \times 10^8$, $p = 2$. Although the uncertainty on the distance affects the values of some parameters (e.g. R, b_{is}, and total power), it is interesting to note that the suggested model of an electron accelerator embedded in the intense stellar radiation field, which has been injecting a power-law type spectrum for the past few 10^5 yrs, can naturally account for the observed gamma-ray spectrum, without violating the constraints derived from X-ray and radio observations. Furthermore, the rather long injection time favours acceleration in stellar winds of, for example, Wolf-Rayet stars over acceleration in supernova remnants. A leptonic scenario of gamma-ray production requires only a moderate fraction (~1%) of the kinetic power of the stellar winds to be channelled into the acceleration of a non-thermal particle population. Hadronic models, on the other hand, need a rather high ambient gas density in order to keep the required efficiency below unity. The model presented here can be improved further by including a more realistic mixture of different temperature photon fields with different spatial extensions as observed in the vicinity of Wd-2 (including a dust component and later-type stars present in the system). However, it already allows order of magnitude predictions of the flux to be tested in a range accessible to the GLAST experiment.

Acknowledgements. D.H. and K.M. acknowledge the support of the Eberhard Karls Universität Tübingen. This research has made use of NASA's Astrophysics Data System.

Appendix A: Characteristic cooling and escape functions

The integrals in Eqs. (23) and (24) can be rewritten as

$$\tau(\gamma',\gamma) = \frac{8\epsilon_{eff}}{b_s}\int_{\sqrt{1+4\epsilon_{eff}\gamma}}^{\sqrt{1+4\epsilon_{eff}\gamma'}} \frac{\omega^{1-2\beta}\,d\omega}{(\omega^2-1)^2\,(\omega^{-2\beta}+b_{is})} = \frac{8\epsilon_{eff}}{b_s}\left[T_\beta\left(\sqrt{1+4\epsilon_{eff}\gamma'}\right) - T_\beta\left(\sqrt{1+4\epsilon_{eff}\gamma}\right)\right] \quad (A.1)$$

and

$$\lambda(\gamma',\gamma) = 2b_{es}\int_{\sqrt{1+4\epsilon_{eff}\gamma}}^{\sqrt{1+4\epsilon_{eff}\gamma'}} \frac{\omega^{1-2\beta}\,d\omega}{(\omega^2-1)\,(\omega^{-2\beta}+b_{is})} = 2b_{es}\left[\Lambda_\beta\left(\sqrt{1+4\epsilon_{eff}\gamma'}\right) - \Lambda_\beta\left(\sqrt{1+4\epsilon_{eff}\gamma}\right)\right] \quad (A.2)$$

where the indefinite integrals $T_\beta(\omega)$ and $\Lambda_\beta(\omega)$ can be expressed in terms of elementary functions for (negative) integer and half-integer values of β.

In the case of black-body target photons, as well as for power-law photons with index $\alpha_0 < -0.5$, and $\alpha_0 > 1$, one has $\beta = -3/2$ and finds for $b_{is} \neq 1$:

$$\begin{aligned} T_{-3/2}(\omega) = {} & a^{(1)}_{-3/2}\ln(\omega_1^2 - b_{is}^{1/3}\omega_1 + b_{is}^{2/3}) \\ & + a^{(2)}_{-3/2}\arctan\left(\frac{2\omega_1 - b_{is}^{1/3}}{\sqrt{3}b_{is}^{1/3}}\right) + a^{(3)}_{-3/2}\ln(\omega_1 + b_{is}^{1/3}) \\ & + a^{(4)}_{-3/2}\ln(\omega_1+1) \\ & + a^{(5)}_{-3/2}\ln(\omega_1-1) + a^{(6)}_{-3/2}(\omega_1-1)^{-1} \\ & + a^{(7)}_{-3/2}(\omega_1+1)^{-1}, \end{aligned} \quad (A.3)$$

where

$$\begin{aligned} a^{(1)}_{-3/2}(b_{is}) &= -b_{is}^{2/3}(2b_{is}^2 + b_{is}^{8/3} - 6b_{is}^{4/3} + 2b_{is}^{2/3} + 1)/6(b_{is}^2-1)^2, \\ a^{(2)}_{-3/2}(b_{is}) &= -b_{is}^{2/3}(2b_{is}^2 - b_{is}^{8/3} - 2b_{is}^{2/3} + 1)/\sqrt{3}(b_{is}^2-1)^2, \\ a^{(3)}_{-3/2}(b_{is}) &= b_{is}^{2/3}(2b_{is}^2 + b_{is}^{8/3} + 3b_{is}^{4/3} + 2b_{is}^{2/3} + 1)/3(b_{is}^2-1)^2, \\ a^{(4)}_{-3/2}(b_{is}) &= -3b_{is}/4(b_{is}-1)^2 \\ a^{(5)}_{-3/2}(b_{is}) &= 3b_{is}/4(b_{is}+1)^2, \\ a^{(6)}_{-3/2}(b_{is}) &= -1/4(b_{is}+1), \\ a^{(7)}_{-3/2}(b_{is}) &= -1/4(b_{is}-1). \end{aligned}$$

And for $b_{is} = 1$,

$$\begin{aligned} T_{-3/2}(\omega) = {} & -\frac{1}{9}\ln(\omega^2-\omega+1) + \frac{5}{144}\ln(\omega+1) + \frac{3}{16}\ln(\omega-1) \\ & + \frac{1}{24}\frac{\omega^2-7\omega-6}{(\omega+1)^2(\omega-1)}. \end{aligned} \quad (A.4)$$

For the indefinite integral $\Lambda_{-3/2}(\omega)$, one finds for $b_{is} \neq 1$

$$\begin{aligned} \Lambda_{-3/2}(\omega) = {} & c^{(1)}_{-3/2}\ln(\omega^2 - b_{is}^{1/3}\omega + b_{is}^{2/3}) \\ & + c^{(2)}_{-3/2}\arctan\left(\frac{2\omega - b_{is}^{1/3}}{\sqrt{3}b_{is}^{1/3}}\right) + c^{(3)}_{-3/2}\ln(\omega + b_{is}^{1/3}) \\ & + c^{(4)}_{-3/2}\ln(\omega+1) \\ & + c^{(5)}_{-3/2}\ln(\omega-1), \end{aligned} \quad (A.5)$$

where

$$
\begin{aligned}
c^{(1)}_{-3/2}(b_{\rm is}) &= [(2b_{\rm is}^{2/3}-1)b_{\rm is}^{4/3}-b_{\rm is}^{2/3})]/6(b_{\rm is}^2-1),\\
c^{(2)}_{-3/2}(b_{\rm is}) &= (b_{\rm is}^{4/3}-b_{\rm is}^{2/3})/\sqrt{3}(b_{\rm is}^2-1),\\
c^{(3)}_{-3/2}(b_{\rm is}) &= [(b_{\rm is}^{2/3}+1)b_{\rm is}^{4/3}+b_{\rm is}^{2/3})]/3(b_{\rm is}^2-1),\\
c^{(4)}_{-3/2}(b_{\rm is}) &= -1/2(b_{\rm is}-1),\\
c^{(5)}_{-3/2}(b_{\rm is}) &= 1/2(b_{\rm is}+1),
\end{aligned}
$$

and, for $b_{\rm is}=1$:

$$
\begin{aligned}
\Lambda_{-3/2}(\omega) &= \frac{1}{6}\ln(\omega^2-\omega+1)+\frac{1}{3\sqrt{3}}\arctan\left(\frac{2\omega-1}{\sqrt{3}}\right)\\
&\quad+\frac{5}{12}\ln(\omega+1)+\frac{1}{4}\ln(\omega-1)+\frac{1}{6}(\omega+1)^{-1}. \quad \text{(A.6)}
\end{aligned}
$$

In the case of a power-law distribution of target photons with $-0.5<\alpha_0<1$, closed-form expressions of the integrals can be found for the special cases $\alpha_0=0$ and $\alpha_0=1/2$, corresponding to $\beta=-1$ and $\beta=-1/2$, respectively. For $\beta=-1$,

$$
\begin{aligned}
T_{-1}(\omega) &= -\frac{b_{\rm is}}{2(1+b_{\rm is})^2}\ln(\omega^2+b_{\rm is})+\frac{b_{\rm is}}{2(1+b_{\rm is})^2}\ln(\omega^2-1)\\
&\quad-\frac{1}{2(b_{\rm is}+1)}(\omega^2-1)^{-1}, \quad \text{(A.7)}\\
\Lambda_{-1}(\omega) &= \frac{b_{\rm is}}{2(1+b_{\rm is})}\ln(\omega^2+b_{\rm is})+\frac{1}{2(1+b_{\rm is})}\ln(\omega^2-1). \quad \text{(A.8)}
\end{aligned}
$$

whereas for $\beta=-1/2$ one has for $b_{\rm is}\neq 1$

$$
\begin{aligned}
T_{-1/2}(\omega) &= a^{(1)}_{-1/2}\ln(\omega+b_{\rm is})+a^{(2)}_{-1/2}\ln(\omega+1)+a^{(3)}_{-1/2}\ln(\omega-1)\\
&\quad+a^{(4)}_{-1/2}(\omega+1)^{-1}+a^{(5)}_{-1/2}(\omega-1)^{-1}, \quad \text{(A.9)}
\end{aligned}
$$

where

$$
\begin{aligned}
a^{(1)}_{-1/2}(b_{\rm is}) &= b_{\rm is}^2/(b_{\rm is}^2-1)^2,\\
a^{(2)}_{-1/2}(b_{\rm is}) &= -b_{\rm is}/4(b_{\rm is}-1)^2,\\
a^{(3)}_{-1/2}(b_{\rm is}) &= b_{\rm is}/4(b_{\rm is}+1)^2,\\
a^{(4)}_{-1/2}(b_{\rm is}) &= -1/4(b_{\rm is}-1),\\
a^{(5)}_{-1/2}(b_{\rm is}) &= -1/4(b_{\rm is}+1)
\end{aligned}
$$

and, for $b_{\rm is}=1$:

$$
\begin{aligned}
T_{-1/2}(\omega) &= -\frac{1}{16}\ln(\omega+1)+\frac{1}{16}\ln(\omega-1)\\
&\quad+\frac{1}{8}\frac{\omega^2-3\omega-2}{(\omega+1)^2(\omega-1)}. \quad \text{(A.10)}
\end{aligned}
$$

Similarly, for the function $\Lambda_{-1/2}$ we find, for $b_{\rm is}\neq 1$:

$$
\Lambda_{-1/2}(\omega)=c^{(1)}_{-1/2}\ln(\omega+b_{\rm is})+c^{(2)}_{-1/2}\ln(\omega+1)+c^{(3)}_{-1/2}\ln(\omega-1), \quad \text{(A.11)}
$$

where

$$
\begin{aligned}
&c^{(1)}_{-1/2}(b_{\rm is})=b_{\rm is}^2/(b_{\rm is}^2-1), \qquad c^{(3)}_{-1/2}(b_{\rm is})=1/2(b_{\rm is}+1),\\
&c^{(2)}_{-1/2}(b_{\rm is})=-1/2(b_{\rm is}-1).
\end{aligned}
$$

And, finally, for $b_{\rm is}=1$:

$$
\Lambda_{-1/2}(\omega)=\frac{3}{4}\ln(\omega+1)+\frac{1}{4}\ln(\omega-1)+\frac{1}{2}(\omega+1)^{-1}. \quad \text{(A.12)}
$$

Appendix B:

For the case where accelerated particles start to inject from the central source at time t_0 with a power-law type finite energy spectrum:

$$
Q=\begin{cases} Q_0\gamma^{-p} & \text{for } \gamma_{\rm min}\le\gamma\le\gamma_{\rm max}\\ 0 & \text{otherwise,}\end{cases} \quad \text{(B.1)}
$$

undergoing synchrotron and inverse Compton losses in the Thomson regime, $\dot\gamma=(b_s+b_{\rm iC})\gamma^2\equiv b\gamma^2$, and escaping from the system (with radius R) at a rate $\nu_{\rm esc}=b_{\rm esc}\gamma$ (see Sect. 2.2), the solution of Eq. (1) splits into two branches, depending on whether the maximum injected energy, $\gamma_{\rm max}$, has had enough time to "cool down" to a value γ_1 lower or higher than the minimum injected energy, $\gamma_{\rm min}$.

If $\gamma_{\rm min}<\gamma_1$, then the solution reads:

$$
N(\gamma,t)=\begin{cases}
0, & \gamma<\gamma_2\\
K\gamma^{-(p+1)}\left\{\left(\frac{\gamma}{\gamma_{\rm min}}\right)^q-[1-b\gamma(t-t_0)]^q\right\}, & \gamma_2\le\gamma\le\gamma_{\rm min}\\
K\gamma^{-(p+1)}\{1-[1-b\gamma(t-t_0)]^q\}, & \gamma_{\rm min}<\gamma<\gamma_1\\
K\gamma^{-(p+1)}\left[1-(\frac{\gamma}{\gamma_{\rm max}})^q\right], & \gamma_1\le\gamma\le\gamma_{\rm max}\\
0, & \gamma>\gamma_{\rm max}
\end{cases} \quad \text{(B.2)}
$$

If $\gamma_{\rm min}>\gamma_1$, one gets:

$$
N(\gamma,t)=\begin{cases}
0, & \gamma<\gamma_2\\
K\gamma^{-s}\left\{\gamma_{\rm min}^{-q}-\left[\gamma^{-1}-b(t-t_0)\right]^q\right\}, & \gamma_2\le\gamma\le\gamma_1\\
K\gamma^{-s}(\gamma_{\rm min}^{-q}-\gamma_{\rm max}^{-q}), & \gamma_1<\gamma<\gamma_{\rm min}\\
K\gamma^{-(p+1)}\left[1-(\frac{\gamma}{\gamma_{\rm max}})^q\right], & \gamma_{\rm min}\le\gamma\le\gamma_{\rm max}\\
0, & \gamma>\gamma_{\rm max}
\end{cases} \quad \text{(B.3)}
$$

where $q=p-1+b_{\rm esc}/b$, $K=Q_0/bq$, $s=2-b_{\rm esc}/b$ and the values of γ_1 and γ_2 are given by Eqs. (14) and (15), respectively.

Appendix C: Inverse Compton and synchrotron emissivities

The spectrum of photons scattered by an energetic electron from an isotropic photon gas that follows a differential photon number density $\mathrm{d}n=n(\epsilon)\mathrm{d}\epsilon$ was derived e.g. by Blumenthal & Gould (1970) in the head-on collision approximation and is given by their Eq. (2.48):

$$
\frac{\mathrm{d}N_{\gamma,\epsilon}}{\mathrm{d}t\mathrm{d}\epsilon_1}=\frac{3\sigma_T mc^3}{\gamma}\frac{n(\epsilon)\mathrm{d}\epsilon}{\epsilon}\cdot f(q) \quad \text{(C.1)}
$$

with

$$
f(q)=2q\ln q+(1+2q)(1-q)+\frac{1}{2}\frac{(4\epsilon\gamma/mc^2)^2}{1+4q\epsilon\gamma/mc^2}(1-q) \quad \text{(C.2)}
$$

and

$$
q=\frac{\epsilon_1}{4\epsilon\gamma/mc^2(1-\epsilon_1)}. \quad \text{(C.3)}
$$

The total inverse Compton spectrum from a distribution of electrons $dN = N(\gamma)d\gamma$ follows from the integration over ϵ and γ:

$$\frac{dN_{IC}}{d\epsilon_1 dt} = \int d\epsilon \int d\gamma N(\gamma) \frac{dN_{\gamma,\epsilon}}{dt d\epsilon_1}. \quad (C.4)$$

The emitted synchrotron power per unit frequency interval emitted by a single electron with pitch angle α and magnetic field B is given e.g. by Ginzburg & Syrovatskii (1964)

$$j(\nu) = \frac{\sqrt{3}e^3 B \sin\alpha}{mc^2} F\left(\frac{\nu}{\nu_c}\right) \quad (C.5)$$

with the critical frequency

$$\nu_c = \gamma^2 \frac{3eB\sin\alpha}{4\pi mc} \quad (C.6)$$

and

$$F(x) = x \int_x^\infty dt K_{5/3}(t). \quad (C.7)$$

A simple approximation of $F(x)$ was used for the calculations presented in this paper (see e.g. Melrose 1980):

$$F(x) = 1.85 x^{1/3} \exp(-x). \quad (C.8)$$

This approximation provides a relative accuracy that is better than 1 per cent in the region of the maximum at $x \sim 0.29$ and still reasonable accuracy in the broad range of $0.1 \leq x \leq 10$. The luminosity-per-unit-frequency interval from an electron distribution $dN = N(\gamma)d\gamma$ is calculated by integration over γ:

$$J(\nu) = \int d\gamma N(\gamma) j(\nu). \quad (C.9)$$

We assume an isotropic magnetic field such that $\sin\alpha = \sqrt{2/3}$.

References

Abdo, A. A., Allen, B., Berley, D., et al. 2007, ApJ, 658, L33
Aharonian, F., Akhperjanian, A., Beilicke, M., et al. 2002, A&A, 393, L37
Aharonian, F., Akhperjanian, A., Beilicke, M., et al. 2005a, A&A, 431, 197
Aharonian, F., Akhperjanian, A. G., Aye, K.-M., et al. 2005b, Science, 309, 746
Aharonian, F., Akhperjanian, A. G., Aye, K.-M., et al. 2005c, A&A, 442, 1
Aharonian, F., Akhperjanian, A. G., Bazer-Bachi, A. R., et al. 2007, A&A, 467, 1075
Albert, J., Aliu, E., Anderhub, H., et al. 2006, Science, 312, 1771
Anchordoqui, L. A., Beacom, J. F., Butt, Y. M., et al. 2007a, ArXiv e-prints, 706
Anchordoqui, L. A., Beacom, J. F., Goldberg, H., Palomares-Ruiz, S., & Weiler, T. J. 2007b, Phys. Rev. Lett., 98, 121101
Ascenso, J., Alves, J., Beletsky, Y., & Lago, M. T. V. T. 2007, A&A, 466, 137
Bednarek, W. 2007, ArXiv e-prints, 704
Blumenthal, G. R. 1971, Phys. Rev. D, 3, 2308
Blumenthal, G. R., & Gould, R. J. 1970, Rev. Mod. Phys., 42, 237
Churchwell, E., Whitney, B. A., Babler, B. L., et al. 2004, ApJS, 154, 322
Coppi, P. S. 1992, MNRAS, 258, 657
Dame, T. M. 2007, ArXiv e-prints, 707
Dermer, C. D., & Atoyan, A. M. 2002, ApJ, 568, L81
Felten, J. E., & Morrison, P. 1966, ApJ, 146, 686
Ginzburg, V. L., & Syrovatskii, S. I. 1964, The Origin of Cosmic Rays (New York: Macmillan, 1964)
Goldwurm, A., Caraveo, P. A., & Bignami, G. F. 1987, ApJ, 322, 349
Hinton, J. A., & Aharonian, F. A. 2007, ApJ, 657, 302
Horns, D., Hoffmann, A. I. D., Santangelo, A., Aharonian, F. A., & Rowell, G. P. 2007, A&A, 469, L17
Jones, F. C. 1965, Phys. Rev., 137, 1306
Kardashev, N. S. 1962, AZh, 39, 393
Katarzyński, K., Ghisellini, G., Svensson, R., & Gracia, J. 2006, A&A, 451, 739
Khangulyan, D., Hnatic, S., & Aharonian, F. 2007, Ap&SS, 212
Kirk, J. G., Ball, L., & Skjaeraasen, O. 1999, Astropart. Phys., 10, 31
Krawczynski, H., Coppi, P. S., & Aharonian, F. 2002, MNRAS, 336, 721
Kusunose, M., & Takahara, F. 2005, ApJ, 621, 285
Lightman, A. P., & Zdziarski, A. A. 1987, ApJ, 319, 643
Maeder, A., & Meynet, G. 1987, A&A, 182, 243
Mastichiadis, A. & Kirk, J. G. 1997, A&A, 320, 19
Melrose, D. B. 1980, Plasma astrophysics: Nonthermal processes in diffuse magnetized plasmas, Astrophysical applications (New York, Gordon and Breach Science Publishers), 2, 430
Moderski, R., Sikora, M., Coppi, P. S., & Aharonian, F. 2005a, MNRAS, 364, 1488
Moderski, R., Sikora, M., Coppi, P. S., & Aharonian, F. 2005b, MNRAS, 363, 954
Murata, K., Tamaki, H., Maki, H., & Shibazaki, N. 2003, PASJ, 55, 473
Neronov, A., & Chernyakova, M. 2006, ArXiv Astrophysics e-prints
Rauw, G., Manfroid, J., Gosset, E., et al. 2007, A&A, 463, 981
Stawarz, Ł. & Kirk, J. G. 2007, ApJ, 661, L17
Sturner, S. J., Skibo, J. G., Dermer, C. D., & Mattox, J. R. 1997, ApJ, 490, 619
Tang, S., & Wang, Q. D. 2005, ApJ, 628, 205
Torres, D. F., Domingo-Santamaría, E., & Romero, G. E. 2004, ApJ, 601, L75
Townsley, L., Feigelson, E., Montmerle, T., et al. 2005, in X-Ray and Radio Connections, ed. L. O. Sjouwerman & K. K Dyer, published electronically by NRAO, `http://www.aoc.nrao.edu/events/xraydio`, held 3–6 February 2004 in Santa Fe, New Mexico, USA
Völk, H. J. 2006, in IAU Symp. 230, Populations of High Energy Sources in Galaxies, ed. E. J. A. Meurs & G. Fabbiano, 95
Whiteoak, J. B. Z., & Uchida, K. I. 1997, A&A, 317, 563
Zdziarski, A. A. 1989, ApJ, 342, 1108